VIP Single-Molecule Junctions Very Important Paper

How to cite: *Angew. Chem. Int. Ed.* **2021**, *60*, 12274–12278
International Edition: doi.org/10.1002/anie.202100168
German Edition: doi.org/10.1002/ange.202100168

Atomically Precise Engineering of Single-Molecule Stereoelectronic Effect

Linan Meng[+], Na Xin[+], Jinying Wang[+], Jiyu Xu, Shizhao Ren, Zhuang Yan, Miao Zhang, Cheng Shen, Guangyu Zhang, Xuefeng Guo, and Sheng Meng**

Abstract: *Charge transport in a single-molecule junction is extraordinarily sensitive to both the internal electronic structure of a molecule and its microscopic environment. Two distinct conductance states of a prototype terphenyl molecule are observed, which correspond to the bistability of outer phenyl rings at each end. An azobenzene unit is intentionally introduced through atomically precise side-functionalization at the central ring of the terphenyl, which is reversibly isomerized between trans and cis forms by either electric or optical stimuli. Both experiment and theory demonstrate that the azobenzene side-group delicately modulates charge transport in the backbone via a single-molecule stereoelectronic effect. We reveal that the dihedral angle between the central and outer phenyl ring, as well as the corresponding rotation barrier, is subtly controlled by isomerization, while the behaviors of the phenyl ring away from the azobenzene are hardly affected. This tunability offers a new route to precisely engineer multi-configurational single-molecule memories, switches, and sensors.*

Single-molecule electronics has drawn extensive attentions from a variety of research fields because of potential applications in integrated circuits[1] and strong ability to unveil the hidden physical properties of materials at the atomic scale.[2] In general, the conductance characteristics are mainly determined by the coupling strength (including linkage coupling and center molecular coupling)[3] and the injection gap (the energy offset between the dominant conducting molecular orbitals and the electrode's Fermi level).[1i,4] In addition, the subtle difference in molecular conformations can result in distinguishable conductance states because of device sensitivity,[5] reaching a single-molecule and single-event precision. Introducing external atoms or groups at the side-group position, which does not have continuous σ-bonds with the molecular junction, has been reported as an effective method to modulate the electronic or geometric properties of the molecular backbone.[1c,6] This concept lays down the foundation for step-by-step monitoring of chemical reactions and interactions at the single-event level in a dynamic manner, whereas the reaction center was placed at the side-group position.[2a,7]

Based on the graphene-molecule-graphene single-molecule junction (GMG-SMJ) platform,[8] here we present a molecular design by introducing an azobenzene side group at the central ring of terphenyl, which is connected to graphene electrodes through covalent bonds, with *p*-phenylenediamine as the bridge (Figure 1a). These stable covalent bonds at the interface lay the foundation for the following *I–V* and *I–t* measurement. Azobenzene is a well-known photochromic functional group, which can transit between two distinct states (*trans*/*cis*) under optical stimuli of different wavelengths (UV/Vis), as shown in Figure 1b. As reported elsewhere,[1f,2f] we have confirmed that the electric field can effectively modulate the energy alignments among *trans*, *cis* and transition states due to the asymmetric spatial orientation of the azobenzene side group. As a result, the azobenzene unit can isomerize between *trans* (which is more stable in energy) and *cis* forms with the help of the bias electric field. This isomerization is expressed by the conductance sharp jump in Figure 1c at around −0.20 V. The electric field-induced isomerization of azobenzene provides a unique opportunity to study how the side groups control the single-molecule stereoelectronic effect in the terphenyl backbone.

For a bare terphenyl molecular structure, there exist two different configurations with different tilted directions between the outer phenyl rings at each end. The introduction of azobenzene as the side group makes the situation much more complex as demonstrated in Figure 1c, where three

[*] Dr. L. Meng,[+] Dr. J. Xu, Dr. C. Shen, Prof. Dr. G. Zhang, Prof. Dr. S. Meng
Beijing National Laboratory for Condensed Matter Physics
Institute of Physics, Chinese Academy of Sciences
Beijing 100190 (P. R. China)
E-mail: smeng@iphy.ac.cn

Dr. L. Meng,[+] Dr. J. Xu, Dr. C. Shen, Prof. Dr. G. Zhang, Prof. Dr. S. Meng
University of Chinese Academy of Sciences
Beijing 100049 (P. R. China)

Dr. N. Xin,[+] Dr. J. Wang,[+] Dr. S. Ren, Z. Yan, Prof. Dr. X. Guo
Beijing National Laboratory for Molecular Sciences, State Key Laboratory for Structural Chemistry of Unstable and Stable Species
College of Chemistry and Molecular Engineering, Peking University
Beijing 100871 (P. R. China)
E-mail: guoxf@pku.edu.cn

M. Zhang, Prof. Dr. X. Guo
Center of Single-Molecule Sciences, Institute of Modern Optics
College of Electronic Information and Optical Engineering
Nankai University
38 Tongyan Road, Jinnan District, Tianjin 300350 (P. R. China)

Prof. Dr. S. Meng
Key Laboratory of Material Physics, School of Physics and Microelectronics, Zhengzhou University
Zhengzhou 450052 (P. R. China)

[+] These authors contributed equally to this work.

Supporting information and the ORCID identification number(s) for the author(s) of this article can be found under: https://doi.org/10.1002/anie.202100168.

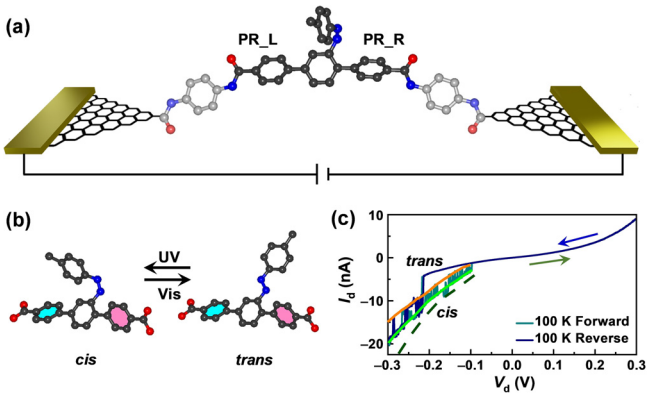

Figure 1. Device geometry and charge transport characteristics. a) Schematic diagram of GMG-SMJs with the target molecule covalently bonded to graphene electrodes. b) The optimized structures of the functional center that can isomerize reversibly between *cis* and *trans* forms. c) Current–voltage curves measured at 100 K. The three sub-states of conductance are labeled with orange, light green and dark green lines. The orange and green curves are simply used to highlight the different conductance states.

obvious conducting sub-states were observed when azobenzene was in the *cis* form. Based on a combined theoretical and experimental approach as detailed below, we demonstrated that the dynamic process of PR_R (the phenyl ring adjacent to the N=N bond) was significantly influenced by the side chain structures. This phenomenon revealed that the rotation barrier of PR_R could be tuned by isomerizing azobenzene. In contrast, the rotation processes of PR_L (the phenyl ring away from the N=N bond) remain nearly unchanged whenever azobenzene was in *trans* or *cis* forms.

To explain the phenomenon observed in Figure 1c, both the conformational changing processes of PR_L and PR_R under the *cis* and *trans* configurations of azobenzene were investigated based on density functional theory (DFT). After structural optimization, four stable conformations of the functional center were found in both *cis* and *trans* forms, respectively, as shown in Figure 2a,c. In comparison with the bare terphenyl (±36°), the dihedral angle of the outer phenyl ring at each end reference to the central ring is different. When azobenzene is in the *cis* form, the twisted angle of PR_L is around ±36°, while that of PR_R are of two different values: −39° (*c*_1 and *c*_2 as shown in Figure 2a) and 43° (*c*_3 and *c*_4 as shown in Figure 2a). When azobenzene is in the *trans* form, the twisted angle of PR_L/PR_R is around ±36°/±46°. As shown in Figure 2c, *t*_1 and *t*_3 (*t*_2 and *t*_4) have a similar geometry due to the planar configuration of *trans*. The precise twisted angle between adjacent phenyl rings are listed in Table S2 of the Supporting Information.

To clarify the thermodynamic processes of conformational changes in both *cis* and *trans* forms, the electron energies of different stable and transition states were calculated (Figure 2b,d), where the energy of each state 1 was used as the reference. In comparison with the rotation barrier in the pure terphenyl molecule (≈7.87 kJ mol^{-1}), PR_L shows a similar value (7.0–8.0 kJ mol^{-1}), while that of PR_R in the *cis* (≈12 kJ mol^{-1}) and *trans* forms (≈23 kJ mol^{-1}) are nearly two and three times higher, respectively. Although the energies of the four states in the *trans* form are close to each other, their transition barriers are large enough (Figure 2d) to separate them (at least into two distinct states). All above information indicates that the steric hindrance of azobenzene has a non-negligible effect on the behaviors of PR_R, which is more significant in the *trans* form than that in the *cis* form, resulting from different spatial and electronic structures in both forms. These theoretical calculations set the foundation for the following measurement of stereoelectronic effect-induced conductance switching.

Here, by taking advantages of the stereoelectronic effect, we aim to explore the azobenzene-controlled temperature-dependent phenyl torsion and corresponding conductance switching. As reported in the previous work,[1f] *cis* and *trans* are the stable form at −0.30 V and 0.30 V, respectively, thanks to the bias electric field effect. Therefore, we chose the bias voltage of −0.30 V and 0.30 V to measure the real-time conductance characteristics under different temperatures.

As demonstrated in Figure 3, four distinct conductance states are observed at 80 K for the *cis* form, which first merge

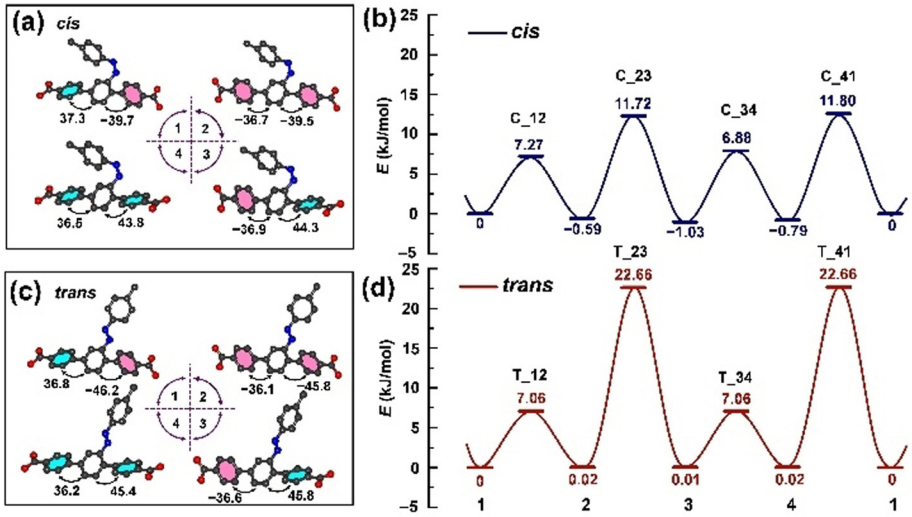

Figure 2. Theoretical calculation of stable conformations and energy profiles. a,c) The molecular structures with different PR_L and PR_R orientations in *cis* (a) and *trans* (c) forms, respectively. By using the central phenyl ring as the reference, anticlockwise rotation of the phenyl ring is fulfilled with pink color and clockwise rotation of the phenyl ring is fulfilled with blue color. Seen from the right side, the clockwise rotation angle is positive and the anticlockwise rotation angle is negative with respect to the central phenyl ring. b,d) Electronic energies (in kJ mol^{-1}) of four stable states for *cis* (blue line) and *trans* isomers (red line), as well as those for the corresponding transition states of the full molecule in Figure 1a. These states are connected to describe the energy barriers needed to overcome during the rotation of phenyl rings.

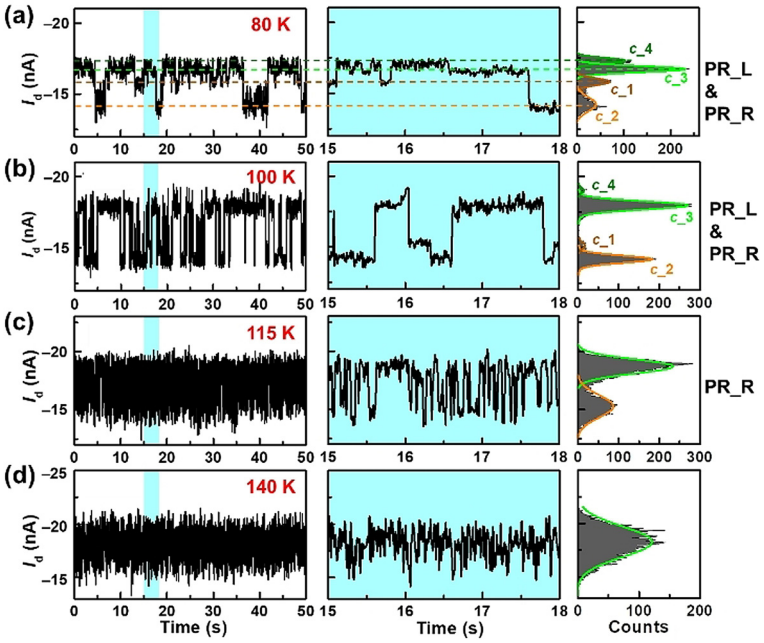

Figure 3. Temperature dependence of *I–t* curves when azobenzene is in the *cis* form. a–d) *I–t* curves at high vacuum environment with different temperatures: 80 K (a), 100 K (b), 115 K (c) and 140 K (d). The bias voltage was set as −0.30 V to fix the azobenzene in the *cis* form. The sampling rate is 10 ms. There are a total of ≈5000 sampling points in each *I–t* curve. For the corresponding histogram, the number of bins is 100. Middle panels are the enlarged *I–t* curves marked in blue, and right panels are the corresponding histograms of currents fitted with a Gaussian function.

into two states as the temperature increases, finally into one conductance state when the temperature reaches 140 K. In contrast, only two conductance states are observed at 80 K for the *trans* form, and then merge into one conductance state, while another two conductance states arise at 115 K (Figure 4).

In our devices, the eight states were achieved by in situ rotation of the phenyl rings and azobenzene. As a result, the coupling between the amide linkage and graphene electrodes for different states of the single molecular device was nearly unchanged.[9] In this case, the junction conductance is dominated by the center molecular coupling and injection gap. Our and other previous works[1e,f,10] demonstrated that the relative energy level of *p*-HOMO of molecular devices tends to be consistent with the HOMO of the center molecules. To determine the correspondence between the conductance states and molecular configurations, it is reasonable to analyze the molecular orbital energies of different molecular configurations. Figure 5a shows the calculated frontier molecular orbital energy. Experimentally, the conductivity from high to low in the *cis* form is $c\_4 > c\_3 > c\_1 > c\_2$ (Figure 3a), consistent with the four distinct HOMO states calculated (Figure 5a). When temperature rises to 100 K as shown in Figure 3b, the conductance states of c_1 and c_2 (c_3 and c_4), though still distinguishable, tend to merge into one, in comparison with that of 80 K. From this point, we can infer that the high (low) conductance state at 115 K originates from the joint contribution of c_3 and c_4 (c_1 and c_2). To gain more information, the mean dwell times of the high and low conductance states at 100 K and 115 K were analyzed. At 100 K, the mean dwell time of the high and low conductance states are ≈149.3 ms and ≈292.2 ms, respectively. In contrast, at 115 K, they are ≈11.4 ms and ≈40.4 ms, respectively. This demonstrates that the switching frequency of the device increases with temperature.

To further understand the temperature-dependent switching behavior of molecular junctions when azobenzene is in the *cis* form, the thermodynamic and kinetic processes of molecular switching were thoroughly analyzed. The thermodynamic equilibrium constant K_{ij}^{c} and reaction rate constant k_{ij}^{c} for the reaction from c_i to c_j (i/j = 1, 2, 3 and 4) can be expressed as $K_{ij}^{c} \propto \exp(-\Delta G_{ij}^{c}/k_B T)$ and $k_{ij}^{c} \propto \exp(-Ea_{ij}^{c}/k_B T)$, respectively, where ΔG is the free energy change, E_a is the activation energy, and T is the temperature. Both the K_{ij}^{c} and k_{ij}^{c} are related with temperature. At 80 K, E_a and thermal energy $k_B T$ ($\approx 0.75\ \mathrm{kJ\,mol^{-1}}$) are at the same order of

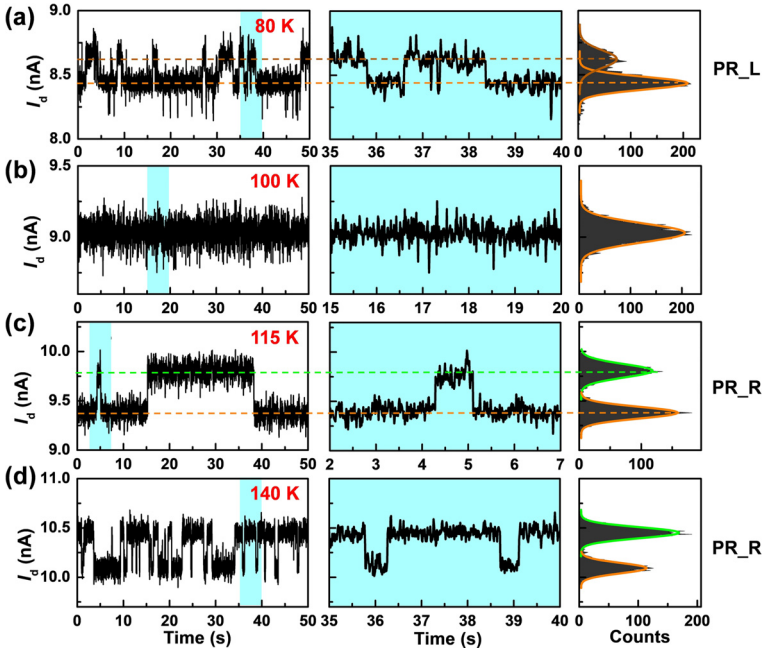

Figure 4. Temperature dependence of *I–t* curves when azobenzene is in the *trans* form. a–d) *I–t* curves in a high vacuum environment with different temperatures: 80 K (a), 100 K (b), 115 K (c) and 140 K (d). The bias voltage was set as 0.30 V to fix the azobenzene in the *trans* form. The sampling rate is 10 ms. There are a total of ≈5000 sampling points in each *I–t* curve. For the corresponding histogram, the number of bins is 100. Middle panels are the enlarged *I–t* curves marked in blue, and right panels are the corresponding histograms of currents fitted with a Gaussian function.

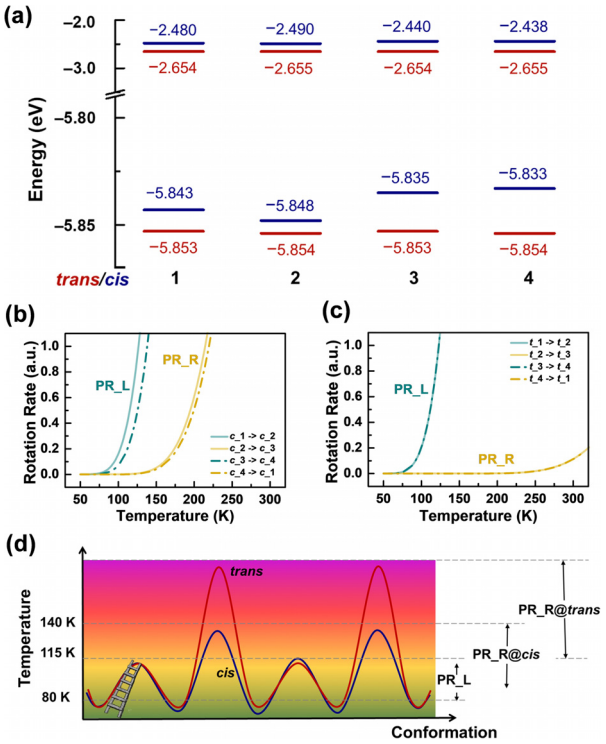

Figure 5. Molecular orbital energies of different molecular configurations. a) Energy levels of the highest occupied molecular orbital (HOMO) and lowest unoccupied molecular orbital (LUMO) for the eight states of the isolated azobenzene-substituted terphenyl molecule. The blue line stands for the *cis* form and the red line for the *trans* form. Since *p*-HOMO is closer to the Fermi level of graphene, *p*-HOMO dominates the junction conductance. The energy difference among the four states in the *cis* form is more severe than that in the *trans* form, resulting in a larger conductance difference for the *cis* form. b,c) The calculated rotation rates between 4 states in the *cis* form and 4 states in the *trans* form as a function of temperature. d) Schematic diagram for the rotation processes of the two phenyl rings at each end as a function of temperature.

magnitude and the ΔG_{ij}^{c} (0.37–0.61 kJ mol^{-1}, Table S3) are lower than $k_B T$, the rotation can happen for the aspect of K_{ij}^{c} and k_{ij}^{c} (Figure 5b; Figure S1). Correspondingly, the conformation changes among *c*_1, *c*_2, *c*_3 and *c*_4 are observed as demonstrated by conductance switching in *I*–*t* plots at 80 K as shown in Figure 3a. Note that the rotation barriers for PR_L and PR_R are different as shown in Figure 2, the reaction rate constant k_{ij}^{c} (switching rate) of PR_L (rotating between *c*_1 and *c*_2 or *c*_3 and *c*_4) is higher than that of PR R (rotating between *c*_2 and *c*_3 or *c*_4 and *c*_1). With increasing the temperature ($T \geq 115$ K), the rotation of PR_L becomes so fast that *c*_1 and *c*_2 (*c*_3 and *c*_4) cannot be distinguished in experiments, which explains why only two conductance states occur at 115 K in Figure 3c. As the temperature rises above 140 K, both PR_L and PR_R rotate so fast that the system reaches its equilibrium quickly. Neither dominating state nor switching process can be observed at high temperatures. Therefore, we can obtain only the statistical average of all four states with averaged conductance, as shown in Figure 3d.

Based on the calculated molecular orbital energies and differences in molecular conjugacy, we conclude that the conductivity of different states in the *trans* form follows the sequence of $t\_2 \leq t\_1 < t\_4 \approx t\_3$, which is consistent with the geometric and energy level analysis of different configurations. Noted that the *trans* form shows two HOMO values differing by $\approx$1 meV, resulting in a smaller difference in injection gap than that in the *cis* form. These theoretical results are consistent with the experiment where the conductance differences among states in the *trans* form are much smaller than that in the *cis* form, as summarized in Table S4. Similar to the analysis on the *cis* form, we determine that the conductance switching in the *trans* form at 80 K (Figure 4a) corresponds to the rotation of PR_L. Different from that in the *cis* form, the Gibbs energy differences of each configuration in *trans* form can be neglected, while the rotation barrier differences between PR_L and PR_R are much larger. Therefore, the temperature at which the reaction rate constants of the switching (corresponding to different phenyl ring rotation) begin to jump is distinct (Figures 5c; Figure S1). When temperature rises to 100 K, PR_L rotates too fast to be resolved in experiments, and only one conductance state was detected. As temperature reaches 115 K, PR_R begins to rotate, resulting in two new conductance states given that the different couplings between the PR_R terphenyl (in two configurations) and the rest of the molecule can result in different p-FMOs due to the changes in molecular conjugacy. With increasing the temperature, the rotation rate increases, accounting for the fact that the switching rate at 140 K is obviously higher than that at 115 K.

The overall processes for phenyl rotation from 80 K to 140 K are summarized in Figure 5d. Because the rotation barrier follows the order PR_R@*trans* > PR_R@*cis* > PR_L (the side chain has little impact on PR_L), the rotation processes of PR_L at both forms of side chain as well as that of PR_R in the *cis* form show up at 80 K. As the temperature increases, the rotation of PR_L is too fast to be resolved in conductance measurements at 115 K, followed by PR_R@*cis* at 140 K. In contrast, the rotation state of PR_R@*trans* can be clearly resolved even at 140 K.

A control measurement on the bare terphenyl molecule (Supporting Information, Figures S2–S5) were performed to further support that the stochastic switching behaviors originates from the rotation of phenyls. We also compare the different discoveries presented in Ref. [1f], Ref. [2a] and the present work. In Ref. [1f], the effects of electric field on the azobenzene isomerization between *trans* and *cis* forms were studied, while here we illustrate how the side-chain azobenzene subtly affects the rotation behavior of phenyl ring of the same molecule in the two conformations (*trans* and *cis* forms), which has never been studied before. The theme of Ref. [2a], on the other hand, is to investigate stochastic transitions of a classical quadrupolar hydrogen bonding system through intermolecular proton transfer and lactam–lactim tautomerism with a single-bond resolution.

In conclusion, we demonstrate that precise tunability of a stereoelectronic effect can be achieved in single-molecule junctions, originating from thermally induced stochastic rotation of phenyl rings in a terphenyl backbone, which is in turn subtly controlled by the azobenzene side group attached to the central ring in either *trans* or *cis* forms. Both experi-

ment and theory show that the phenyl ring close to the substituted position can be affected more significantly than that far away. The introduction of substituent side groups is an efficient method to tune the stereoelectronic effect in molecular junctions, thus providing new insights into constructing functional single-molecule devices, as well as designing organic electronic materials.

Acknowledgements

We acknowledge primary financial supports from the National Natural Science Foundation of China (11934003, 12025407, 21727806, 21933001, 91850120, 11774396), the National Key R&D Program of China (2016YFA0300902 and 2017YFA0204901), Chinese Academy of Sciences (XDB330301), and the Tencent Foundation through the XPLORER PRIZE.

Conflict of interest

The authors declare no conflict of interest.

Keywords: azobenzene · functionalization · rotation barriers · stereoelectronic effects · terphenyl rings

[1] a) D. Xiang, X. Wang, C. Jia, T. Lee, X. Guo, *Chem. Rev.* **2016**, *116*, 4318 – 4440; b) L. Sun, Y. A. Diaz-Fernandez, T. A. Gschneidtner, F. Westerlund, S. Lara-Avila, K. Moth-Poulsen, *Chem. Soc. Rev.* **2014**, *43*, 7378 – 7411; c) N. Xin, J. Guan, C. Zhou, X. Chen, C. Gu, Y. Li, M. A. Ratner, A. Nitzan, J. F. Stoddart, X. Guo, *Nat. Rev. Phys.* **2019**, *1*, 211 – 230; d) N. Xin, X. Li, C. Jia, Y. Gong, M. Li, S. Wang, G. Zhang, J. Yang, X. Guo, *Angew. Chem. Int. Ed.* **2018**, *57*, 14026 – 14031; *Angew. Chem.* **2018**, *130*, 14222 – 14227; e) C. Jia, A. Migliore, N. Xin, S. Huang, J. Wang, Q. Yang, S. Wang, H. Chen, D. Wang, B. Feng, Z. Liu, G. Zhang, D. Qu, H. Tian, M. A. Ratner, H. Q. Xu, A. Nitzan, X. Guo, *Science* **2016**, *352*, 1443 – 1445; f) L. Meng, N. Xin, C. Hu, J. Wang, B. Gui, J. Shi, C. Wang, C. Shen, G. Zhang, H. Guo, S. Meng, X. Guo, *Nat. Commun.* **2019**, *10*, 1450; g) H. Song, Y. Kim, Y. H. Jang, H. Jeong, M. A. Reed, T. Lee, *Nature* **2009**, *462*, 1039 – 1043; h) H. Park, J. Park, A. K. L. Lim, E. H. Anderson, A. P. Alivisatos, P. L. McEuen, *Nature* **2000**, *407*, 57 – 60; i) N. Zhang, W.-Y. Lo, Z. Cai, L. Li, L. Yu, *Nano Lett.* **2017**, *17*, 308 – 312.

[2] a) C. Zhou, X. Li, Z. Gong, C. Jia, Y. Lin, C. Cu, G. He, Y. Zhong, J. Yang, X. Guo, *Nat. Commun.* **2018**, *9*, 807; b) M. H. Garner, H. Li, Y. Chen, T. A. Su, Z. Shangguan, D. W. Paley, T. Liu, F. Ng, H. Li, S. Xiao, C. Nuckolls, L. Venkataraman, G. C. Solomon, *Nature* **2018**, *558*, 415 – 419; c) B.-Y. Choi, S.-J. Kahng, S. Kim, H. Kim, H. W. Kim, Y. J. Song, J. Ihm, Y. Kuk, *Phys. Rev. Lett.* **2006**, *96*, 156106; d) A. Safiei, J. Henzl, K. Morgenstern, *Phys. Rev. Lett.* **2010**, *104*, 216102; e) M. Alemani, M. V. Peters, S. Hecht, K.-H. Rieder, F. Moresco, L. Grill, *J. Am. Chem. Soc.* **2006**, *128*, 14446 – 14447; f) Y. Li, C. Yang, X. Guo, *Acc. Chem. Res.* **2019**, *53*, 159 – 169; g) P. Gehring, J. M. Thijssen, H. S. J. van der Zant, *Nat. Rev. Phys.* **2019**, *1*, 381 – 396; h) T. A. Su, M. Neupane, M. L. Steigerwald, L. Venkataraman, C. Nuckolls, *Nat. Rev. Mater.* **2016**, *1*, 16002; i) J. Henzl, M. Mehlhorn, H. Gawronski, K.-H. Rieder, K. Morgenstern, *Angew. Chem. Int. Ed.* **2006**, *45*, 603 – 606; *Angew. Chem.* **2006**, *118*, 617 – 621; j) T. Hines, I. Diez-Perez, J. Hihath, H. Liu, Z.-S. Wang, J. Zhao, G. Zhou, K. Müllen, N. Tao, *J. Am. Chem. Soc.* **2010**, *132*, 11658 – 11664; k) L. Lafferentz, F. Ample, H. Yu, S. Hecht, C. Joachim, L. Grill, *Science* **2009**, *323*, 1193 – 1197.

[3] a) Kim, J. M. Beebe, Y. Jun, X. Y. Zhu, C. D. Frisbie, *J. Am. Chem. Soc.* **2006**, *128*, 4970 – 4971; b) N. A. Bruque, R. R. Pandey, R. K. Lake, *Phys. Rev. B* **2007**, *76*, 205322; c) C.-C. Kaun, T. Seideman, *Phys. Rev. B* **2008**, *77*, 033414.

[4] a) C. Bruot, J. Hihath, N. Tao, *Nat. Nanotechnol.* **2012**, *7*, 35 – 40; b) L. Venkataraman, Y. S. Park, A. C. Whalley, C. Nuckolls, M. S. Hybertsen, M. L. Steigerwald, *Nano Lett.* **2007**, *7*, 502 – 506.

[5] a) A. C. Aragonès, N. Darwish, J. Im, B. Lim, J. Choi, S. Koo, I. Díez-Pérez, *Chem. Eur. J.* **2015**, *21*, 7716 – 7720; b) M. C. Walkey, C. R. Peiris, S. Ciampi, A. C. Aragones, R. B. Domínguez-Espíndola, D. Jago, T. Pulbrook, B. W. Skelton, A. N. Sobolev, I. D. Perez, M. J. Piggott, G. A. Koutsantonis, N. Darwish, *ACS Appl. Mater. Interfaces* **2019**, *11*, 36886 – 36894.

[6] a) W.-Y. Lo, N. Zhang, Z. Cai, L. Li, L. Yu, *Acc. Chem. Res.* **2016**, *49*, 1852 – 1863; b) C. M. Guédon, H. Valkenier, T. Markussen, K. S. Thygesen, J. C. Hummelen, S. J. van der Molen, *Nat. Nanotechnol.* **2012**, *7*, 305 – 309.

[7] a) J. Guan, C. Jia, Y. Li, Z. Liu, J. Wang, Z. Yang, C. Gu, D. Su, K. N. Houk, D. Zhang, X. Guo, *Sci. Adv.* **2018**, *4*, eaar2177; b) C. Gu, C. Hu, Y. Wei, D. Lin, C. Jia, M. Li, D. Su, J. Guan, A. Xia, L. Xie, A. Nitzan, H. Guo, X. Guo, *Nano Lett.* **2018**, *18*, 4156 – 4162; c) H. Wen, W. Li, J. Chen, G. He, L. Li, M. A. Olson, A. C. H. Sue, J. F. Stoddart, X. Guo, *Sci. Adv.* **2016**, *2*, e1601113.

[8] a) Y. Cao, S. Dong, S. Liu, L. He, L. Gan, X. Yu, L. L. Steigerwald Michael, X. Wu, Z. Liu, X. Guo, *Angew. Chem. Int. Ed.* **2012**, *51*, 12228 – 12232; *Angew. Chem.* **2012**, *124*, 12394 – 12398; b) C. Jia, B. Ma, N. Xin, X. Guo, *Acc. Chem. Res.* **2015**, *48*, 2565 – 2575; c) N. Xin, J. Wang, C. Jia, Z. Liu, X. Zhang, C. Yu, M. Li, S. Wang, Y. Gong, H. Sun, G. Zhang, Z. Liu, G. Zhang, J. Liao, D. Zhang, X. Guo, *Nano Lett.* **2017**, *17*, 856 – 861.

[9] X. Yin, Y. Zang, L. Zhu, J. Z. Low, Z.-F. Liu, J. J. B. Neaton, L. Venkataraman, L. M. Campos, *Sci. Adv.* **2017**, *3*, eaao2615.

[10] a) C. Jia, J. Wang, C. Yao, Y. Cao, Y. Zhong, Z. Liu, Z. Liu, X. Guo, *Angew. Chem. Int. Ed.* **2013**, *52*, 8666 – 8670; *Angew. Chem.* **2013**, *125*, 8828 – 8832; b) C. Guédon, H. Valkenier, T. Markussen, K. Thygesen, J. Hummelen, S. van der Molen, *Nat. Nanotechnol.* **2012**, *7*, 305 – 309; c) C. R. Arroyo, S. Tarkuc, R. Frisenda, J. S. Seldenthuis, C. H. M. Woerde, R. Eelkema, F. C. Grozema, H. S. J. van der Zant, *Angew. Chem. Int. Ed.* **2013**, *52*, 3152 – 3155; *Angew. Chem.* **2013**, *125*, 3234 – 3237; d) T. A. Su, H. Li, M. L. Steigerwald, L. Venkataraman, C. Nuckolls, *Nat. Chem.* **2015**, *7*, 215 – 220.

Manuscript received: January 5, 2021
Accepted manuscript online: March 2, 2021
Version of record online: April 26, 2021

